coatings

Communication

High-Performance Pure Aluminum Coatings on Stainless Steels by Cold Spray

Jialin Fan [1,2,3,†], Haitao Yun [4,†], Xiaoqiang Zhang [1,2], Dongxu Chang [1], Xin Chu [2,*], Yingchun Xie [2,*] and Guosheng Huang [3,*]

1 School of Materials Science and Engineering, Shenyang University of Technology, Shenyang 110870, China
2 National Engineering Laboratory of Modern Materials Surface Engineering Technology, Guangdong Provincial Key Laboratory of Modern Surface Engineering Technology, Institute of New Materials, Guangdong Academy of Sciences, Guangzhou 510650, China
3 State Key Laboratory for Marine Corrosion and Protection, Luoyang Ship Material Research Institute (LSMRI), Qingdao 266237, China
4 Aecc South Industry Co., Ltd., Zhuzhou 412002, China
* Correspondence: xin.chu@hotmail.com (X.C.); xieyingchun@gdinm.com (Y.X.); huanggs@sunrui.net (G.H.)
† These authors contributed equally to this work.

Abstract: Aluminum target material is an important target material and is widely used in preparations of semiconductor films, integrated circuits, display circuits, protective films, decorative films, etc. In this study, pure aluminum coatings were deposited on stainless steel substrates by cold-spray technology as part of an overall project to produce large-size pure aluminum sputtering target materials. The results show that pure aluminum coatings exhibit high adhesive strength (~98 MPa), high deposition efficiency (~95%), and low porosity (~0.3%) on stainless steel substrates. The bonding mechanisms of pure aluminum coatings on stainless steel are a combination of metallurgical and mechanical interlocking. The evolutions of microstructure and mechanical properties of pure aluminum coatings under different heat treatments were also studied. With the increase of heat treatment temperature, it is found that cold-sprayed aluminum coatings become more homogenous in microstructure, the microhardness is reduced, and the adhesive strength seems to be slightly reduced. Overall, this study demonstrates significant advantages of cold-spray technology in depositing high-performance pure aluminum coatings on stainless steels.

Keywords: cold spraying; aluminum; stainless steel; bond strength; heat treatment

Citation: Fan, J.; Yun, H.; Zhang, X.; Chang, D.; Chu, X.; Xie, Y.; Huang, G. High-Performance Pure Aluminum Coatings on Stainless Steels by Cold Spray. *Coatings* **2023**, *13*, 738. https://doi.org/10.3390/coatings13040738

Academic Editor: Cecilia Bartuli

Received: 9 March 2023
Revised: 27 March 2023
Accepted: 3 April 2023
Published: 4 April 2023

1. Introduction

Aluminum target material is an important target material and has a wide range of applications in preparations of semiconductor films, integrated circuits, display circuits, protective films, decorative films, etc. [1–4]. With the development of the market industry, the requirements for the quality of aluminum targets are also increasing. In order to prevent fracture or rupture in the target preparation or transportation process, the target is usually connected to a stainless-steel backing tube, which improves the mechanical properties of the target and also ensures good electrical contact with the target. The traditional methods of joining aluminum with stainless steel include overlay welding and thermal spraying. The overlay-welding process is tedious and costly. The heat input is large and easily produces lots of welding slag and flying chips [5–7]. The thermal-spraying processes, such as HVOF, are mature technology and have benefits such as unrestricted workpiece size and high efficiency; however, due to the high process temperature, metallic elements are easy to oxidize, the coating porosity is relatively high, the microstructural uniformity is poor due to local corrosion, and thick deposits are difficult due to large residual stresses [8–12]. At present, it is still difficult to prepare high-quality, high-bond-strength pure aluminum coatings directly on stainless steel surfaces.

In recent years, cold-spray technology has developed rapidly and has wide application prospects in the fields of advanced functional coatings and additive manufacturing [13–19]. The main advantages of cold-spray technology are as follows: (1) the particle temperature is below melting point, and therefore it can effectively avoid oxidation and phase transformation and retain the high purity of feedstock materials; (2) low thermal effect, high adhesive strength, and high coating density of the deposits; (3) high powder deposition efficiency (DE), high deposition rate, and thick coatings can be obtained. In the literature, there are a few studies on cold spraying pure aluminum on different substrates (e.g., Mg alloys and Al alloys) and their properties. For instance, Bu et al. [20] reported dense and thick cold-sprayed aluminum coatings on AZ91D Mg substrates and found that the coating adhesion strength decreases after heat treatment due to the formation of a brittle Al_3Mg_2 intermetallic layer. Blochet et al. [21] investigated the effect of surface treatment on the bond strength of cold-sprayed pure aluminum coatings on aluminum alloys and showed that the bond strength can reach ~35 MPa with the use of coarse grit sandblasting, which is 40% higher than non-blasted or blasted with fine grits aluminum coatings, indicating that substrate surface roughness has a significant effect on particle adhesion. However, there are few works in the literature on the cold spraying of pure aluminum coating on stainless steel surfaces. Due to the high hardness and high strain-hardening rate of stainless steel, it is generally considered difficult to directly deposit aluminum particles onto it ("soft on hard" mode) by using cold spray due to the lack of substrate deformation [22]. In this study, cold-spray technology was used to assess the feasibility of depositing pure aluminum coatings directly onto stainless steels, and the microstructure, mechanical properties, and the effects of heat treatment on the above metrics were studied.

2. Materials and Methods

2.1. Experimental Materials

The substrate material was 304 stainless steel plates with the size of 100 mm × 100 mm × 1.8 mm. The substrate surface was slightly polished with #180 sandpaper, ultrasonicated to remove surface dirt, rinsed with acetone, and then blown dry. The feedstock powder was pure aluminum powder (XCLL401.1, Institute of New Materials, Guangdong Academy of Sciences). Figure 1a,b show the Scanning Electron Microscope (SEM) morphology of Al powders at 500× and 2000× magnifications. Most of the powder particles have high sphericity, with a small number of irregular satellite particles being present. The particle size distribution of the Al powder measured by a laser particle size analyzer is shown in Figure 1c. The particle size range is Dv (10) 15.4 μm, Dv (50) 25.0 μm, and Dv (90) 44.4 μm.

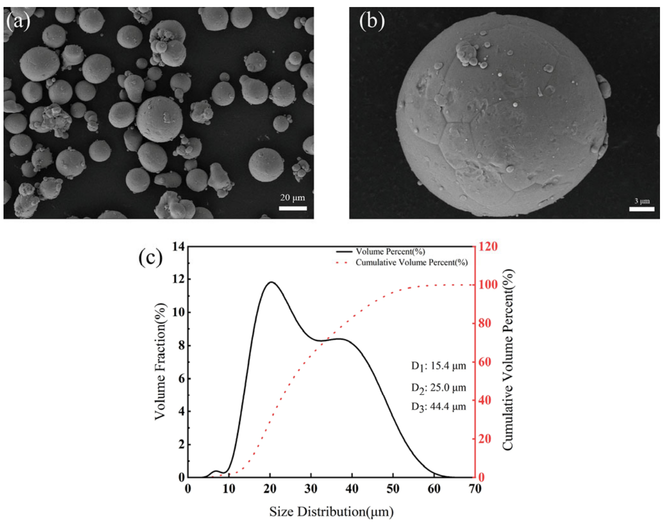

Figure 1. (**a**) 500× SEM, (**b**) 2000× SEM, and (**c**) particle size distribution of the Al powder.

2.2. Coating Preparation

The coating deposition was carried out using a high-pressure cold-spraying system PCS 800 (Plasma Giken Co., Ltd., Hiroshima, Japan), which is located at the Institute of New Materials, Guangdong Academy of Sciences. A plastic nozzle was used which was specifically designed to deposit pure aluminum coatings. Nitrogen was used as the carrier gas. The gas pressure and temperature are two key process parameters for cold spray. In previous trial tests, we studied a wide range of process parameters to cover the entire spraying window of aluminum on stainless steel. Therefore, in this study, we report only the four representative parameters and the deposit performance. For the ease of comparison, we only vary one parameter in each condition, and the 4# is the highest parameters possible to deposit aluminum without any nozzle-clogging issue. The specific process parameters are shown in Table 1.

Table 1. Process parameters for cold spray of Al powder.

No.	Carrier Gas	Gas Pressure (MPa)	Gas Temperature (°C)	Spray Distance (mm)
1#	N_2	3	400	20
2#	N_2	4	400	20
3#	N_2	5	400	20
4#	N_2	5	600	20

2.3. Sample Characterization

The DE was calculated by the weight of powder deposited on the substrate divided by the weight of powder over the substrate. The coating cross-sections were observed using an optical microscope and a field-emission SEM (Gemini SEM300, ZEISS, Jena, Germany). The coating porosity was determined according to the ASTM E2109 standard and was calculated using ImageJ software. The coatings were also etched by Keller's reagent for 15 s to reveal the particle boundaries and grain features. The coating microhardness was measured using a Vickers microhardness tester with a load of 50 g and loading time of 15 s.

In this study, the coating bond strength was measured using two different methods. The first is the usual ASTM C633-2013 method in which coating specimens were sectioned into 25.4 mm diameter cylinders. Then the specimen and the counterpart were glued together with E7 epoxy resin adhesive and then cured at 110 °C for 4 h in fixture; after that, tensile tests were carried out using a universal testing machine (GP-TS2000M, Gopoint, Shenzhen, China). However, this method can be limited by the strength of the epoxy itself (the specified maximum strength of E-7 epoxy adhesive is ~70–80 MPa, and such values also depend on coating materials being tested, surface conditions, curing process, etc.). The second method is a micro-tensile setup reported by our group previously, which was designed to measure the bonding strength of highly adhesive coatings, as shown in Figure 2. In the test, cylinders with the same material as the substrate are machined into the special geometry, as shown in Figure 2a. The coating is then deposited onto the substrate, and then the entire setup is subjected to tension pull-off tests. The failure at the interface is considered to be the coating bond strength and is then calculated as the force (F) divided by the area of the conical end surface.

After the cold-spraying treatment, a heat treatment was also carried out in and argon-atmosphere-protected tube furnace, and samples were heated to 300 °C, 400 °C, and 500 °C and held for 4 h. After the heat treatment, the coatings were etched to show the microstructure, and the microhardness and bonding strength of the coating were characterized.

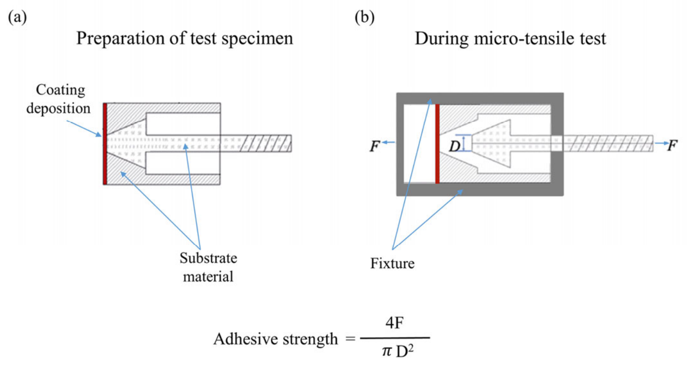

Figure 2. Schematic of the micro-tensile test: (**a**) coating is deposited on the test assembly made of substrate material, (**b**) micro-tensile test is carried out to pull the test assembly apart.

3. Results and Discussion

3.1. Microstructure and Microhardness

Figure 3 shows cross-sectional microstructures of pure aluminum coatings that were cold sprayed at different parameters. At lower parameters (3 MPa 400 °C), there are a few visible pores and defects in the coating. With the increase of gas pressure and temperature, the number and size of pores and defects within the coatings are significantly reduced. The 4# coating (5 MPa 600 °C) is almost dense and free from obvious defects. It is also observed that the interfaces between pure aluminum coatings and stainless steel substrates are continuous and intimate in all scenarios. There are no obvious defects such as cracks and oxides observed, and the substrate is barely deformed at all parameters.

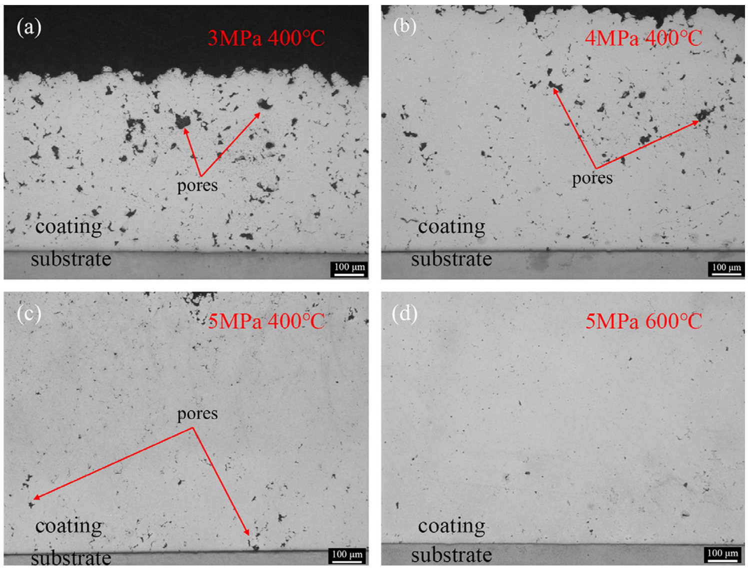

Figure 3. Cross-sectional microstructure of cold-sprayed Al coatings. (**a**) 3 MPa 400 °C; (**b**) 4 MPa 400 °C; (**c**) 5 MPa 400 °C; (**d**) 5 MPa 600 °C.

The gas temperature and pressure are two key factors that affect the in-flight speed of particles. The higher the pressure and temperature, the faster the in-flight speed of particles. Therefore, higher particle velocity and, thus, higher kinetic energy promote the plastic deformation of particles, enabling the particles to elongate into an oblate shape along the vertical direction of spraying; therefore, particle–substrate interfaces are continuously closely bonded, and the as-sprayed coatings are dense [23,24].

The coating porosity was characterized, and the results are shown in Figure 4a. The coating porosity of 1# is ~5.33%, the coating porosity of 2# is ~2.42%, the coating porosity of 3# is ~0.83%, and the coating porosity of 4# is as low as ~0.26%. The coating porosity is consistent with Figure 4a, and it monotonically decreases with the increase of the process parameters. The porosity of the coating is one of the important indicators of the performance of cold-sprayed coatings. Generally speaking, the lower the porosity, the higher the bond strength of the coating. Moreover, to obtain a better sputtering performance for the aluminum target, lower porosity of the coating is preferred.

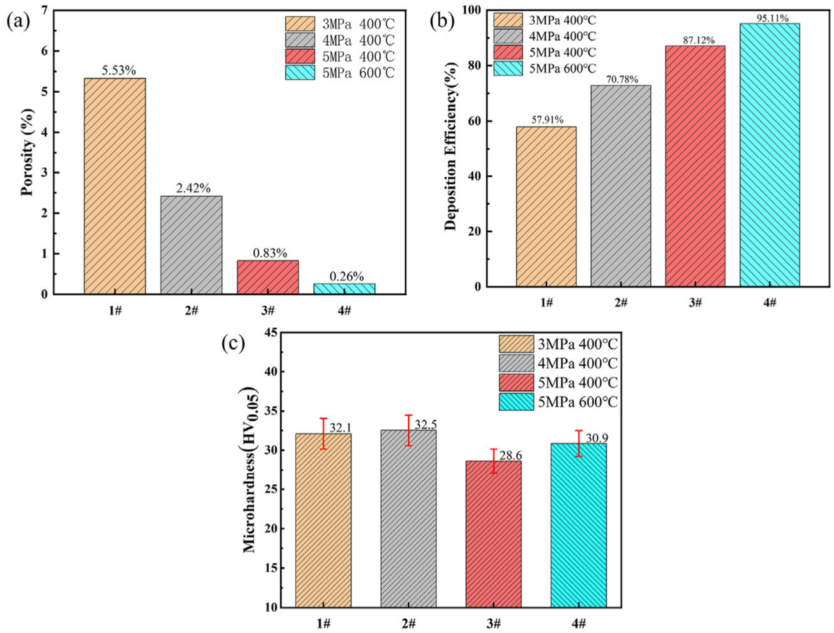

Figure 4. Key metrics of cold-sprayed Al coatings: (**a**) porosity, (**b**) deposition efficiency, and (**c**) microhardness.

The DE results were measured and are shown in Figure 4b. DE indicates the ease with which a powder can be deposited by cold spray. A higher DE for a powder would significantly increase the production efficiency and cost-effectiveness during production. The results show that the DE of Al powder increases with the increase of process parameters. The highest DE of Al powder on 304 stainless steel is 95.11% at process parameters of 5 MPa and 600 °C.

Figure 4c shows the Vickers microhardness of pure aluminum coatings that were cold sprayed under different parameters. The hardness of the 1# coating is 32.1 ± 1.96 $HV_{0\cdot05}$, the hardness of the 2# coating is 32.5 ± 1.81 $HV_{0\cdot05}$, the hardness of the 3# coating is 28.6 ± 1.50 $HV_{0\cdot05}$, and the hardness of the 4# coating is 30.9 ± 1.64 $HV_{0\cdot05}$. For reference, the Vickers microhardness of aluminum powder, as measured, is ~23 $HV_{0\cdot01}$. Hence, the cold-sprayed aluminum coating is a more work-hardened state compared with the Al powder. It is also noted that the coating hardness at higher parameters is lower than it is at lower parameters. Generally, with the increase of gas pressure and temperature, powder particles could achieve higher in-flight velocity, leading to higher particle plastic deformation and more pronounced work-hardening effects [25]. This abnormal phenomenon should indicate that dynamic recrystallization of Al powder occurred at higher process parameters [26].

3.2. Bond Strength

As the key mechanical property index of the coating, the bonding strength determines the service performance and application range of cold-sprayed coatings. The bonding-strength results of the pure aluminum coatings on the 304 stainless steel substrate are reported in Figure 5a. The bond strength was firstly measured by ASTM C633-2013 standard, and all glue failures were observed, as shown in Figure 5b. The bonding strength of the 1# coating is 33 ± 7 MPa, that of the 2# coating is 45 ± 7 MPa, that of the 3# coating is 50 ± 8 MPa, and that of the 4# coating is 68 ± 7 MPa. Although glue failure is not the true coating bonding strength, these results still could be indicative of the relative coating adhesive strength based on our previous experience with pure aluminum coatings. Moreover, to obtain the true adhesive strength, the modified micro-tensile tests were performed to the strongest adhesive coating, #4. The micro-tensile setup is shown in Figure 5c, and the adhesive strength of the 4# coating, as measured, is as high as 98 ± 5 MPa.

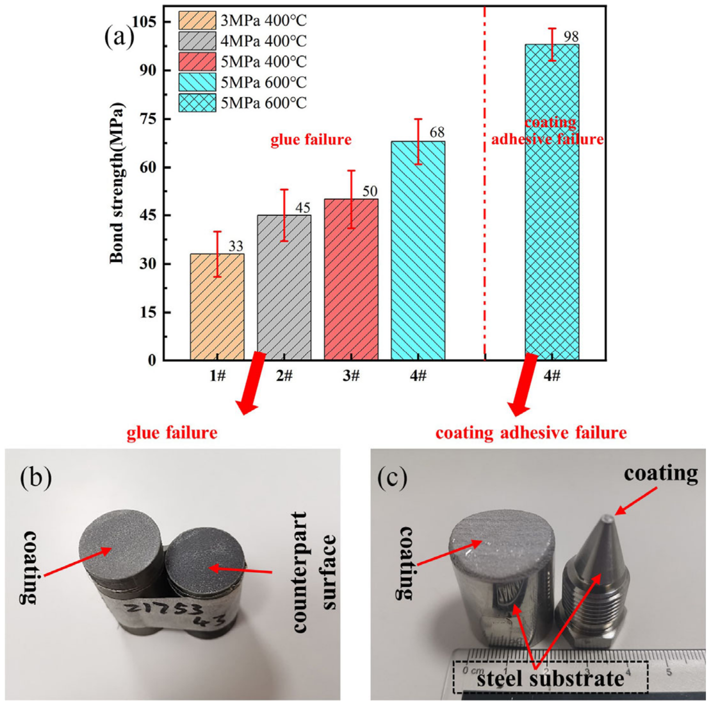

Figure 5. Bond strength results (**a**) and different testing methods of cold sprayed Al coatings: (**b**) ASTM C633 standard, (**c**) micro-tensile test.

To identify the bonding mechanisms of cold-sprayed Al powder on 304 stainless steel, the failure region after the micro-tensile tests was characterized. Figure 6 shows SEM images of the tensile failure section of the 4# coating at the substrate side, and Figure 6b,c show the EDS elemental mapping. The results show there is a certain amount of Al residuals (44.19% in area) on the failed surface, and the substrate surface seems smooth and barely deformed after deposition. Thus, it is reasonable to estimate that strong metallurgical bonding occurred to Al residuals on the stainless steel surface (44.19%), while the rest of the Al coating remained in a state of mechanical interlocking.

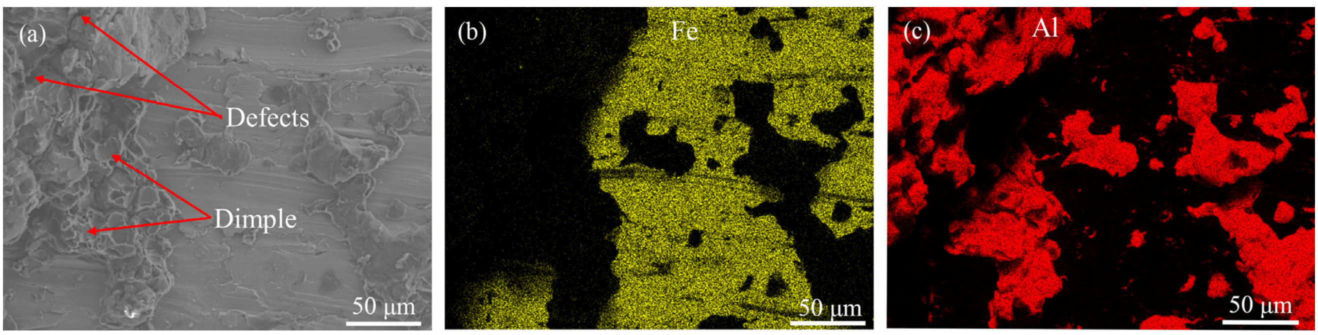

Figure 6. Fracture morphology of cold-sprayed Al coating: (**a**) SEM and (**b**,**c**) EDS (yellow, Fe; red, Al).

3.3. Heat Treatment

Considering that the #4 coating has the best overall performance, it was then subjected to heat-treatment studies. Figure 7 shows the etched-coating microstructure after different heat treatments. In Figure 7a, when the coating is at the as-sprayed state (RT), the particles are visibly severely deformed, and numerous particle–particle interfaces are clear and obvious. With the increase of heat treatment temperature (300 °C to 500 °C), the coating gradually becomes more homogenous, and the particle–particle interface gradually disappears. This is due to the diffusion of the Al element at evaluated temperatures to minimize the surface energy by "healing" the interfaces. However, at 500 °C (Figure 7d), there seems to be obvious phase or defect formation (in dark contrast) along the coating–substrate interface, and this is discussed in the next section.

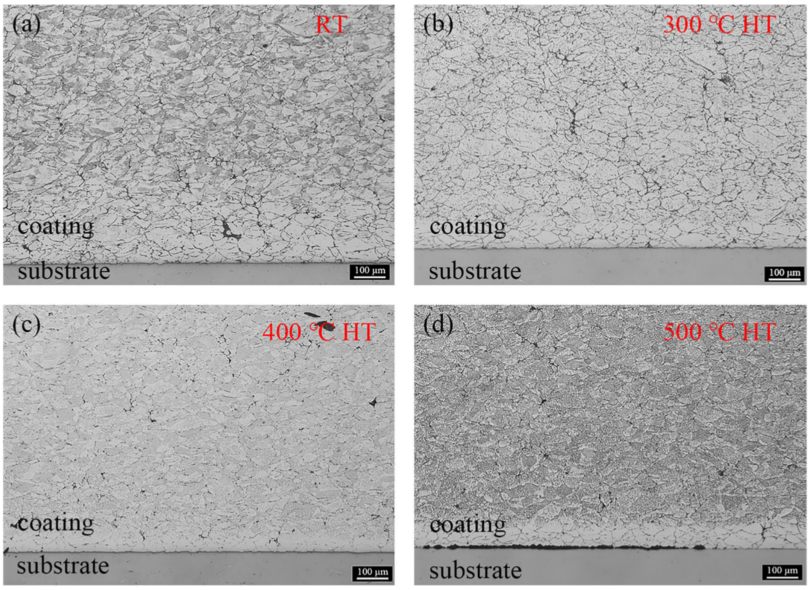

Figure 7. As-etched microstructure of Al coatings: (**a**) RT, (**b**) 300 °C HT, (**c**) 400 °C HT, and (**d**) 500 °C HT.

Figure 8a shows the microhardness of the #4 coating after heat treatment. In general, the coating hardness decreases continuously with the increasing heat-treatment temperature. The hardness of the coating after 4 h of the 500 °C heat treatment is almost identical to that of aluminum powder. The decrement of coating hardness after heat treatment is the combined effect of the release of residual stress, elimination of dislocation density by recovery and recrystallization, grain growth, etc. [27].

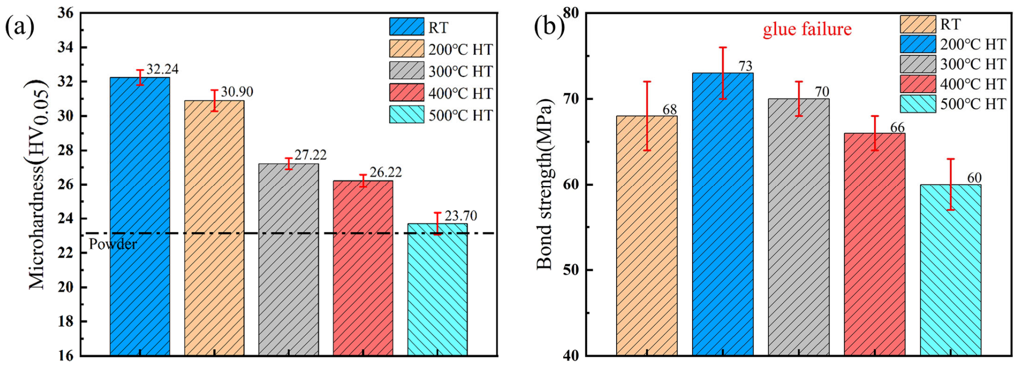

Figure 8. Mechanical properties of Al coatings after heat treatment: (**a**) microhardness and (**b**) bonding strength.

Figure 8 shows the effect of heat treatment on bonding strength, using ASTM C633-2013. Again, the failure mode for all coatings is glue failure. Glue failure means that, after tensile tests, the fracture occurs within the epoxy; thus, the actual coating strength should be higher than the measured value. However, based on our previous experience, such results are still representative of the relative coating bonding strength. The results show that the bonding strength increases slightly with a 200 °C heat treatment and then gradually decreases with the increase of the heat-treatment temperature. The slight increase of the coating bonding strength appears due to the recover phenomenon to release the internal stress. At higher temperatures, as shown in Figure 9, the interdiffusion layer between Al and stainless steel becomes obvious, as well as defects, e.g., cracks at the diffusion layer/Al coating side, and this is speculated to explain the gradual decrease of the coating's bonding strength.

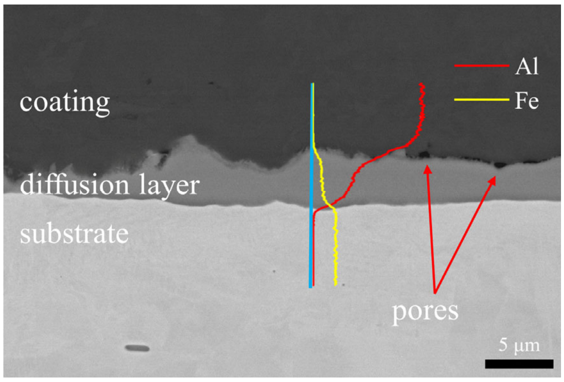

Figure 9. Diffusion layer after heat treatment at 500 °C.

4. Conclusions

In this study, cold-spray technology was used to deposit pure aluminum powder onto a stainless steel substrate as part of an overall project to prepare a large-size aluminum target. Parametric studies were carried out, and the coating microstructure and mechanical properties were characterized. The main conclusions are as follows:

(1) Using N_2 as the carrier gas, pure aluminum coatings with excellent interfacial bonding were successfully prepared on the 304 stainless steel surface. The coating has good overall performance under the process parameters of 5 MPa 600 °C, the bonding strength is ~98 MPa, the DE is ~95%, and the coating porosity is ~0.3%.

(2) With the increase of heat treatment temperature, the cold-sprayed aluminum coating becomes more homogenous in the microstructure, its microhardness is reduced, and the adhesive strength seems to be slightly reduced.

Author Contributions: Conceptualization, J.F. and H.Y.; methodology, D.C. and H.Y.; data curation, J.F. and X.Z.; writing—original draft preparation, J.F.; writing—review and editing, Y.X. and X.C.; supervision, Y.X. and X.C.; project administration, H.Y.; funding acquisition, Y.X. and G.H. All authors have read and agreed to the published version of the manuscript.

Funding: The authors gratefully acknowledge the financial support from the Guangdong Academy of Sciences Special Fund for Comprehensive Industrial Technology Innovation Center Building (No. 2022GDASZH-2022010107), International Cooperation Platform of Science and Technology, Guangdong Academy of Sciences (2022GDASZH-2022010203-003), Key-Area Research and Development Program of Guangdong Province (No. 2020B0101330001), Science Center for Gas Turbine Project (P2022-B-IV-011-001), Guangdong Provincial Key Laboratory of Modern Surface Engineering Technology (No. 2020B1212060049),Research Fund of State Key Laboratory for Marine Corrosion and Protection of Luoyang Ship Material Research Institute (LSMRI) under the contract No. 6142901200303.

Institutional Review Board Statement: Not applicable.

Informed Consent Statement: Not applicable.

Data Availability Statement: Data are contained within the article.

Acknowledgments: The authors would like to thank Liang Zeng and Yunda Nong from the Institute of New Materials, Guangdong Academy of Sciences, for cold spraying experiments. The authors also thank Xundong Sun for his assistance in the experiments and Pengyuan Diao and Yi Wu for their valuable comments.

Conflicts of Interest: The authors declare no conflict of interest.

References

1. Barajas-Valdes, U.; Suárez, O.M. Nanomechanical properties of thin films manufactured via magnetron sputtering from pure aluminum and aluminum-boron targets. *Thin Solid Film.* **2020**, *693*, 137670. [CrossRef]
2. Warren, T.L. The effect of target inertia on the penetration of aluminum targets by rigid ogive-nosed long rods. *Int. J. Impact Eng.* **2016**, *91*, 6–13. [CrossRef]
3. Tang, E.; Zhao, L.; Han, Y.; Chen, C.; Chang, M. Research on the electromagnetic propagating characteristics of hypervelocity impact on the target with aperture and different potential conditions. *Aerosp. Sci. Technol.* **2020**, *107*, 106274. [CrossRef]
4. Rajesh Kumar, B.; Hymavathi, B.; Subba Rao, T. XRD and AFM Studies on Nanostructured Zinc Aluminum Oxide Thin Films Prepared by Multi-Target Magnetron Sputtering. *Mater. Today Proc.* **2017**, *4*, 8638–8644. [CrossRef]
5. Patil, U.S.; Kadam, M.S. Microstructural analysis of SMAW process for joining stainless steel 304 with mild steel 1018 and parametric optimization by using response surface methodology. *Mater. Today Proc.* **2021**, *44*, 1811–1815. [CrossRef]
6. Li, Z.X.; Zhang, L.M.; Ma, A.L.; Hu, J.X.; Zhang, S.; Daniel, E.F.; Zheng, Y.G. Comparative study on the cavitation erosion behavior of two different rolling surfaces on 304 stainless steel. *Tribol. Int.* **2021**, *159*, 106994. [CrossRef]
7. Liao, H.; Zhang, W.; Xie, H.; Li, X.; Zhang, Q.; Wu, X.; Tian, J.; Wang, Z. Effects of welding speed on welding process stability, microstructure and mechanical performance of SUS304 welded by local dry underwater pulsed MIG. *J. Manuf. Process.* **2023**, *88*, 84–96. [CrossRef]
8. Bai, M.; Reddy, L.; Hussain, T. Experimental and thermodynamic investigations on the chlorine-induced corrosion of HVOF thermal sprayed NiAl coatings and 304 stainless steels at 700 °C. *Corros. Sci.* **2018**, *135*, 147–157. [CrossRef]
9. Gorlach, I.A. A new method for thermal spraying of Zn–Al coatings. *Thin Solid Film.* **2009**, *517*, 5270–5273. [CrossRef]
10. Gibbons, G.J.; Hansell, R.G. Thermal-sprayed coatings on aluminium for mould tool protection and upgrade. *J. Mater. Process. Technol.* **2008**, *204*, 184–191. [CrossRef]
11. Sun, B.; Fukanuma, H.; Ohno, N. Study on stainless steel 316L coatings sprayed by a novel high pressure HVOF. *Surf. Coat. Technol.* **2014**, *239*, 58–64. [CrossRef]
12. Han, M.-S.; Woo, Y.-B.; Ko, S.-C.; Jeong, Y.-J.; Jang, S.-K.; Kim, S.-J. Effects of thickness of Al thermal spray coating for STS 304. *Trans. Nonferrous Met. Soc. China* **2009**, *19*, 925–929. [CrossRef]
13. Yin, S.; Suo, X.; Guo, Z.; Liao, H.; Wang, X. Deposition features of cold sprayed copper particles on preheated substrate. *Surf. Coat. Technol.* **2015**, *268*, 252–256. [CrossRef]
14. Srikanth, A.; Mohammed Thalib Basha, G.; Venkateshwarlu, B. A Brief Review on Cold Spray Coating Process. *Mater. Today Proc.* **2020**, *22*, 1390–1397. [CrossRef]
15. Bagherifard, S.; Guagliano, M. Fatigue performance of cold spray deposits: Coating, repair and additive manufacturing cases. *Int. J. Fatigue* **2020**, *139*, 105744. [CrossRef]
16. Meng, X.-M.; Zhang, J.-B.; Han, W.; Zhao, J.; Liang, Y.-L. Influence of annealing treatment on the microstructure and mechanical performance of cold sprayed 304 stainless steel coating. *Appl. Surf. Sci.* **2011**, *258*, 700–704. [CrossRef]
17. Coddet, P.; Verdy, C.; Coddet, C.; Debray, F.; Lecouturier, F. Mechanical properties of thick 304L stainless steel deposits processed by He cold spray. *Surf. Coat. Technol.* **2015**, *277*, 74–80. [CrossRef]
18. Meng, X.; Zhang, J.; Zhao, J.; Liang, Y.; Zhang, Y. Influence of Gas Temperature on Microstructure and Properties of Cold Spray 304SS Coating. *J. Mater. Sci. Technol.* **2011**, *27*, 809–815. [CrossRef]
19. Rokni, M.R.; Widener, C.A.; Champagne, V.R. Microstructural stability of ultrafine grained cold sprayed 6061 aluminum alloy. *Appl. Surf. Sci.* **2014**, *290*, 482–489. [CrossRef]
20. Bu, H.; Yandouzi, M.; Lu, C.; Jodoin, B. Post-heat Treatment Effects on Cold-Sprayed Aluminum Coatings on AZ91D Magnesium Substrates. *J. Therm. Spray Technol.* **2012**, *21*, 731–739. [CrossRef]
21. Blochet, Q.; Delloro, F.; N'Guyen, F.; Jeulin, D.; Borit, F.; Jeandin, M. Effect of the Cold-Sprayed Aluminum Coating-Substrate Interface Morphology on Bond Strength for Aircraft Repair Application. *J. Therm. Spray Technol.* **2017**, *26*, 671–686. [CrossRef]
22. Luo, X.-T.; Li, S.-P.; Li, G.-C.; Xie, Y.-C.; Zhang, H.; Huang, R.-Z.; Li, C.-J. Cold spray (CS) deposition of a durable silver coating with high infrared reflectivity for radiation energy saving in the polysilicon CVD reactor. *Surf. Coat. Technol.* **2021**, *409*, 126841. [CrossRef]
23. Levasseur, D.; Yue, S.; Brochu, M. Pressureless sintering of cold sprayed Inconel 718 deposit. *Mater. Sci. Eng. A* **2012**, *556*, 343–350. [CrossRef]
24. Song, X.; Jin, X.-Z.; Zhai, W.; Tan, A.W.-Y.; Sun, W.; Li, F.; Marinescu, I.; Liu, E. Correlation between the macroscopic adhesion strength of cold spray coating and the microscopic single-particle bonding behaviour: Simulation, experiment and prediction. *Appl. Surf. Sci.* **2021**, *547*, 149165. [CrossRef]
25. Xie, Y.; Planche, M.-P.; Raoelison, R.; Hervé, P.; Suo, X.; He, P.; Liao, H. Investigation on the influence of particle preheating temperature on bonding of cold-sprayed nickel coatings. *Surf. Coat. Technol.* **2017**, *318*, 99–105. [CrossRef]

26. Wong, W. *Understanding the Effects of Process Parameters on the Properties of Cold Gas Dynamic Sprayed Pure Titanium Coatings*; McGill University: Montréal, QC, Canada, 2012.
27. Wei, Y.-K.; Luo, X.-T.; Chu, X.; Huang, G.-S.; Li, C.-J. Solid-state additive manufacturing high performance aluminum alloy 6061 enabled by an in-situ micro-forging assisted cold spray. *Mater. Sci. Eng. A* **2020**, *776*, 139024. [CrossRef]